A low cost and large-scale synthesis of 3D photonic crystal with SP2 lattice symmetry

Cite as: AIP Advances **9**, 085206 (2019); https://doi.org/10.1063/1.5113549
Submitted: 05 June 2019 . Accepted: 31 July 2019 . Published Online: 09 August 2019

Mei-Li Hsieh, Shu-Yu Chen, Alex Kaiser, Yang-Jhe Yan, B. Frey, Ishwara Bhat, Rajendra Dahal, Sayak Bhattacharya, Sajeev John, and Shawn-Yu Lin

A low cost and large-scale synthesis of 3D photonic crystal with SP2 lattice symmetry

Cite as: AIP Advances 9, 085206 (2019); doi: 10.1063/1.5113549
Submitted: 5 June 2019 • Accepted: 31 July 2019 •
Published Online: 9 August 2019

Mei-Li Hsieh,[1,2] Shu-Yu Chen,[1] Alex Kaiser,[2] Yang-Jhe Yan,[1] B. Frey,[2] Ishwara Bhat,[3] Rajendra Dahal,[3] Sayak Bhattacharya,[4] Sajeev John,[4] and Shawn-Yu Lin[2,a)]

AFFILIATIONS

[1]Department of Photonics, National Chiao Tung University, Hsinchu 30050, Taiwan
[2]The Future Chips Constellation and the Department of Physics, Applied Physics, and Astronomy, Rensselaer Polytechnic Institute, 110 8th Street, Troy, New York 12180, USA
[3]Electrical Computer Systems Engineering, Rensselaer Polytechnic Institute, Troy, New York 12180, USA
[4]Department of Physics, University of Toronto, 60 St. George Street, Toronto, Ontario M5S 1A7, Canada

[a)]Author to whom correspondence should be addressed. Electronic mail: sylin@rpi.edu

ABSTRACT

In this work, a novel lithographic method is proposed to prepare three-dimensional (3D) photonic crystal (PC) that is different from conventional top-down and bottom-up approaches. The method combines a 2D optical mask and off-the-axis double optical exposures to create a desirable 3D PC structure. Since the method uses only two optical exposures of a photo-resist layer, it is inherently a low-cost, high throughput and wafer-scale lithographic method. The method is implemented to make a slanted post 3D PC having the SP2 lattice symmetry. Three types of SP2 3D PC structures were successfully fabricated with a minimum feature size of d=1.5 μm over a large scale of 8x10 mm^2, without any observable fabrication defects. The SP2 PCs are: (i) SU8 posts in air background, (ii) air pores in CdS background and (iii) Pt coated on SU8 SP2 templates. A spectroscopic study of the SP2 PCs shows select spectral regions of high reflectance, indicating the existence of a photonic stop band. This low-cost and large-scale method could enable broader technological impacts of 3D PC materials in areas such as thermo-photovoltaics and above room-temperature Bose-Einstein Condensation. Furthermore, this off-axis method could lead to the creation of an entirely new class of slanted-rod based photonic crystals, such as topological photonic crystal in 3D.

I. INTRODUCTION

Since the photonic crystal (PC) concept was first introduced in 1987,[1,2] a new era of advanced nano-materials for molding the flow of light on-chip[3–8] and for extreme light trapping[9–12] has begun. The past three decades have seen significant progress in the preparation of PC materials by both the bottom-up and top-down approaches. These approaches include, but are not limited to, self-assembly,[13] and optical and electron-beam lithography methods.[14,15] The self-assembly approach is attractive, as it naturally produces a three-dimensional (3D) lattice structure. However, it provides a limited choice of lattice symmetry and has a relatively short range (<100μm) of lattice structure order. The lithographic approach is also attractive, as it can produce almost any lattice symmetry, and by extension, a large photonic band gap. In 1994, a layer-by-layer, or woodpile, design with diamond symmetry was proposed.[16] It had a complete PBG of ~25% of the midgap frequency[16] and was amendable to micro-electronic processes.[5,17–19] However, due to extensive equipment usage, and the need to perform a lithographic exposure for each layer, this method suffers from low throughput and high cost. This is the major obstacle for a broader technological impact and utilization of 3D PC materials as of today. Clearly, a new solution is needed to overcome the drawbacks of bottom-up and top-down approaches.

The new 3D PC design we adapt is also a representation of the diamond lattice called the SP2 structure.[20] However, as shown in Figure 1(a), the 3D PC is produced by making two sets of interpenetrating rods, one rotated off-axis by −45° (red color) and the

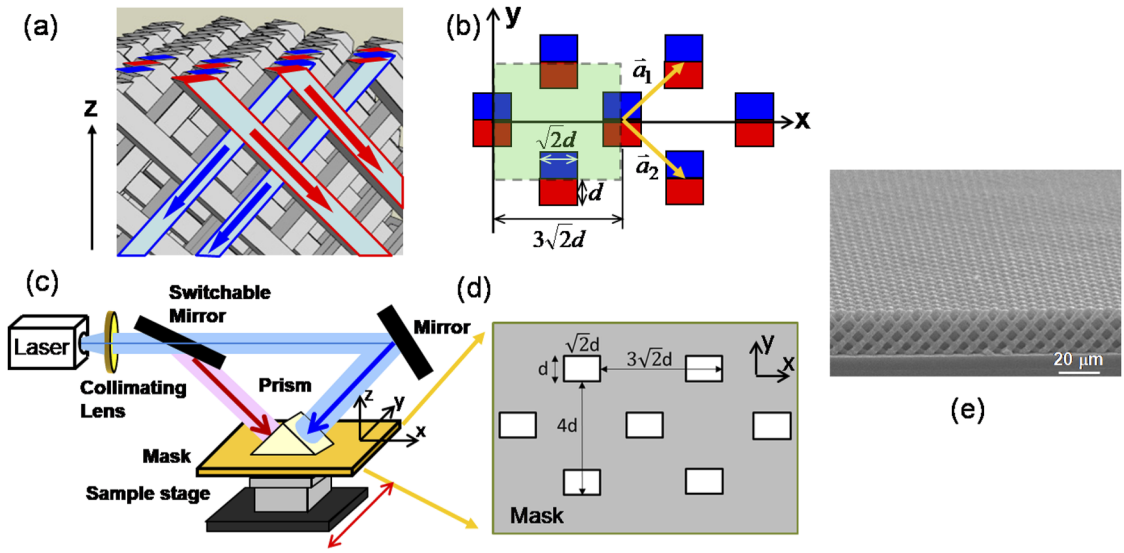

FIG. 1. (a) Schematic of the woodpile SP2 PC structure, consisting of two sets of crossing rods (red and blue arrows); (b) a top view the two sets of rods in the x-y plane; (c) schematic of the optical double exposure lithographic system, where light is to be incident along +45° (the blue arrow path) during the first exposure and, subsequently, −45° (the red arrow path) during the second exposure; (d) the layout of the mask, which is to be shifted along the y-direction during the second exposure; (e) A large area view of the fabricated SP2 PC, demonstrating the structure uniformity over a large area (>100x100μm^2).

other off-axis by +45° (blue color). Figure 1(b) shows a top view of the two sets of crossing rods. Here, one complete cross makes up a unit-cell. Consequently, the task of making a complex 3D structure is transformed into making two sets of linear-rod arrays. This, in turn, simplifies the 3D PC fabrication process. This SP2 PC is important for the realization of the above-room-temperature Bose-Einstein-Condensation due to its reduced symmetry.[21] This SP2 PC may be synthesized by techniques such as direct laser writing,[22,23] ion beam etching[24] and deep x-ray lithography,[25] but each with certain limitations. For example, direct laser writing can produce a precise 3D structure, but is limited to a small sample size of ~50 x 50 x 50 μm^3. Ion-beam etching of GaAs can lead to a large PBG, but the sidewall of the slanted rods tends to be non-straight, due perhaps to ion scattering. Here, we propose a multi-beam laser lithography method[26,27] that would satisfy all the requirements for low cost, large scale, and long-range lattice-order, without sacrificing large photonic band gap.

II. DESIGN OF OPTICAL LITHOGRAPHIC SYSTEM

It is seen in Figure 1(b), that the two sets of crossing rods have an identical 2D triangular pattern, but are shifted relative to each other by a distance *d* along the y-axis. Accordingly, the new optical lithographical system was designed to accommodate (I) an interchangeable optical path (the blue and the red optical paths) by a switchable mirror and (II) an optical mask mounted on a precision translational stage. Figure 1(c) shows a schematic of the optical system. Typically, a UV laser is used to produce a minimum feature size of about one micrometer. Our system uses a λ=355 nm Q-switched laser. Also, a prism is used to guarantee a 45° light path inside the high-index SU8 photo-resist material. A photo of the successfully implemented optical system is shown in the supplemental section. Figure 1(d) shows the detailed design of the 2D triangle mask. Each rectangular hole has dimensions of *d* by $\sqrt{2}$ *d*. The factor of "$\sqrt{2}$" accounts for the geometrical factor of an off-axis 45° light incidence. The lattice constant of the designed SP2 PC is given by $a = 2.9155d$. In a step-by-step procedure, the first exposure of a photoresist layer is done with a light incident angle of −45°, generating the first set of slanted rods (red color). Next, the mask is shifted by a distance "*d*" along the y-axis. Finally, the second exposure is done at +45°, generating the second set of slanted rods (red color). This completes the optical exposure process for generating a SP2 PC structure. We note that, in our experiment, the laser light wavelength is λ=355 nm and the light exposure energy varies from 20–200 mJ/cm^2 depending on the thickness of the photoresist film. Figure 1(e) shows a lower-magnification SEM image of the fabricated structure, demonstrating uniformity over a larger area (>100 x 100 μm^2).

The photosensitive resist we chose is the commercially available, thick film negative photoresist SU8 (MicroChem). In our experiment, a 10–20 μm thick SU8 film is first spin-coated onto a 1 mm-thick silica substrate, and followed by a soft bake. After optical exposure, the resist is baked on a hot plate at 100°C for 2 minutes. This is to promote cross-linkage of the resist to the polymer in the exposed regions. In a subsequent step, the photoresist in the under-exposed regions is washed away by solvent. This completes the fabrication process for the SU8-based SP2 PC structure.

For our SP2 PC, a primary focus of process control is the geometrical shape of the slanted rods. This includes the minimum width, maximum height, tilt angle, and the straightness and relative alignment of the rods. Therefore, a series of experiments were performed to optimize process parameters such as exposure optical intensity and light incident angle. ***First***, a laser beam with

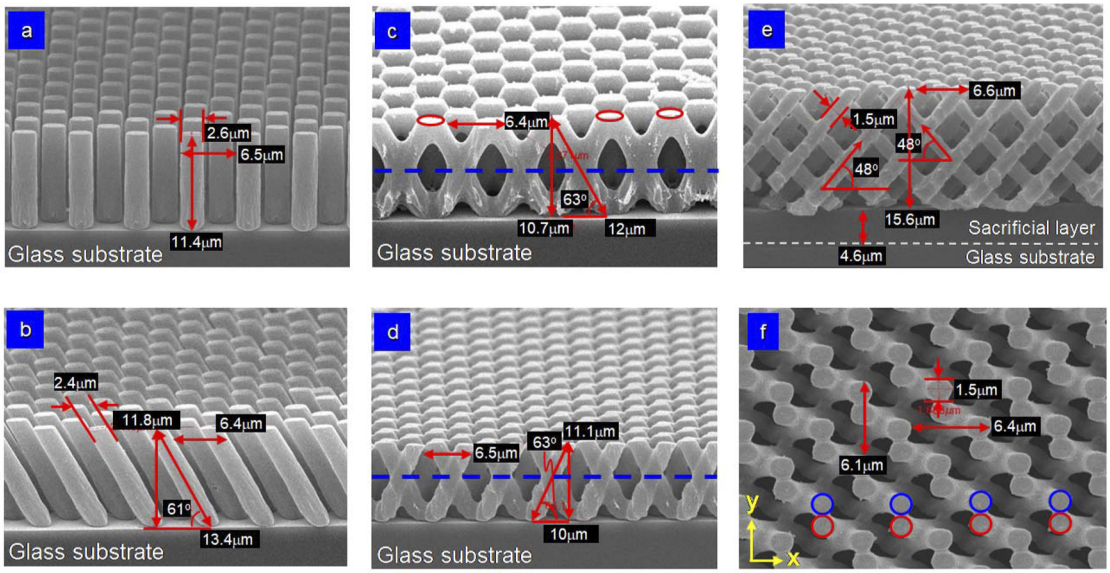

FIG. 2. (a)-(d) are SEM images of the SU8 photoresist PC structure on glass substrate and are exposed without 45-90-45 prism. (a) result of single light exposure at the normal incidence angle; (b) result of single exposure at a slanted incident angle; (c) result of double exposures without shifting the mask. (d) result of double exposure, where the mask is shifted by a distance d along the y-direction. (e) and (f) are the side and top view SEM images of SP2 PC structure, exposed with 45-90-45 prism, respectively.

λ=355 nm was made to impinge the top surface of the mask at normal incidence. We found that a single exposure with a dose of 150 mJ/cm^2 can produce rods with a straight sidewall. Figure 2(a) shows an SEM image of the single exposure result, where the rod height is h = 11.4 μm and the rod width is d = 2.6 μm. During exposure, it is critical that the mask be in direct contact with the top surface of the photoresist. This is to reduce local air-gaps between the mask and the photoresist, and to avoid light diffraction induced by the mask's small feature size. It was further determined that, for laser light of λ=355 nm, it is possible to produce a straight rod of h = 20 μm and d =1.5 μm, having an aspect ratio of >13. ***Second***, we performed an off-axis exposure with the light beam directed at a tilt angle of θ_{air}=45° relative to the surface of the mask in air. However, by Snell's Law, the refracted light inside the SU8 film (refractive index is n =1.6) is expected to be θ_{SU8} = 63.8° relative to the surface of the substrate. Figure 2(b) shows an SEM image of the off-axis, single exposure result, where a set of slanted rods is created and their tilt angle is measured to be θ_{SU8}~61°. Note that, in this off-axis configuration, the optimum dose needed to be increased up to 250 mJ/cm^2 due to a longer optical path length. ***Third***, we performed an off-axis, double exposure calibration. The first exposure was done at θ_{air}=45° through the optical mask and the second at θ_{air}= −45°. Figure 2(c) shows an SEM image of the double-exposure result. In this case, the mask remained un-shifted between the first and the second exposures. Consequently, the two sets of rods formed crosses that overlay with each other. Indeed, the crossing rods at the middle section of the SU8 film (the horizontal blue dashed line) have a good overlapping. This is also evident by observing the top surface image in Figure 2(c), where the two sets of rods join each other at the same location (the red circles). The tilt angle was measured to be θ_{SU8}~63°. ***Fourth***, to create a relative displacement between the two sets of slanted rods, the optical mask was shifted by a distance *d* along the y-axis for the 2nd exposure. Figure 2(d) shows an SEM image of the double-exposure result, with the mask shifted. Due to the mask shifting procedure, the crossing rods at the middle section of the SU8 film (the horizontal blue dashed line) no longer overlap. The tilt angle was measured to be θ_{SU8}~63°. These four steps complete the calibration of the width, straightness, and relative alignment of the slanted rods.

The remaining task is to achieve the designed slanted-rod tilt-angle of θ_{SU8}=45°. However, this desirable angle is not achievable in our current design. This is because, by Snell's law, when light is incident from the air, the critical angle limits the minimum achievable tilt angle inside the SU8 to be θ_{SU8}=48.2°. Here, we use a prism to overcome the problem. The prism is a right-angle prism (45°-90°-45°) with a refractive index of n = 1.6. It is placed in direct contact with the mask, as shown in Figure 1(c). The laser beam is incident normal to the top surface of the prism and propagates without refraction onto the bottom surface of the prism. Hence, we have θ_{prism}=θ_{air}=45°. Since the prism and the SU8 film have the same optical index of n=1.6, no optical refraction is present. Therefore, we can achieve θ_{SU8}=θ_{prism}=45°. Furthermore, to eliminate interface refraction, an index-matching oil (n=1.6) is used to fill the potential air gaps at the following interfaces: one between the prism and the mask, and the other between the mask and the photoresist. Figure 2(e) shows an SEM image of the double-exposure result with the 45°-90°-45° prism in place. The resulting SP2 PC has a tilt angle θ_{SU8}= 48°. This angle is 3° off from the desired 45° and maybe due to a slight mis-alignment of the incident beam relative to the surface normal of the prism or a slight refraction at the prism-SU8 interface. The SP2 PC also a rod-width d = 1.5 μm and a rod height h = 15.6 μm, corresponding to two complete crosses, or two unit

cells. Figure 2(f) shows a top-view SEM image of the SU8 SP2 PC structure. The two sets of slanted rods (indicated by the red and blue circles, respectively) show a precise relative displacement of d = 1.5 μm. This result illustrates the precision of our alignment scheme. Note that our SP2 PC has a typical sample size 8 x 10 mm^2, being limited by the laser beam size. These results demonstrate that our proposed off-axis optical lithographical system can create a nearly ideal SU8-based SP2 3D PC at a large scale using two simple exposure steps.

III. OPTICAL PROPERTIES OF SP2 PC STRUCTURE AND DISCUSSIONS

The optical properties of the successfully fabricated SP2 PC were modeled theoretically and also characterized experimentally. The theoretical modeling of the fabricated samples includes finite-difference-time-domain (FDTD) simulations and frequency-wave vector (f vs k) dispersion calculations.[28] The details are described in the Method section. The theoretical reflectance spectra of the SP2 PCs, computed using FDTD, are compared to the reflectance spectra of the fabricated samples, measured using a combination of Fourier transform infrared (FTIR) spectrometer and infrared microscope. In such an infrared microscope system, light is incident normally onto the sample's surface, is un-polarized and has beam spot size of 100 by 100 μm^2.

Figure 3(a) shows the dispersion diagram of the SP2 PC template (i.e. SU8 posts in air background) for the lowest ten bands

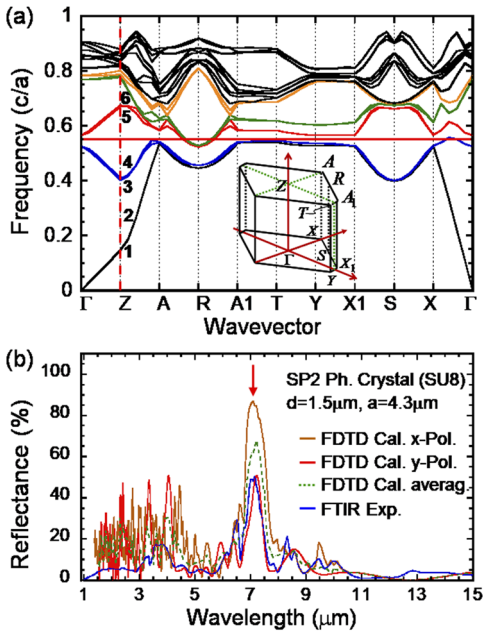

FIG. 3. (a) The frequency vs wavector dispersion curve of our SU8 (post in air background) SP2 PC; (b) Reflectance spectra of the SU8-based SP2 PC with d = 1.5 μm. The experimentally measured curve (blue color) are compared to a FDTD simulation results for x-polarization (brown color), y-polarization (red color), and the averaged one (dashed green color). The reflectance peak at λ = 7.1 μm corresponds to a normalized frequency of 0.61 (c/a).

along the major symmetry points. The inset shows a schematic of the Brillouin zone (BZ) of the SP2 PC. The Γ-Z direction (the vertical, dashed red line) corresponds to light propagation along the sample's surface normal. A large photonic stop band exists along Γ-Z between band 3-4 and band 5-6 for a range of normalized frequency f(c/a) = 0.41–0.67, with a mid-gap frequency $f(c/a)$ = 0.54 (the horizontal solid red line). Here the frequency f is in units of (c/a). Given d =1.5 μm and a = 4.3 μm of our SP2 PC, the expected mid-gap wavelength is $\lambda_{mid\text{-}gap}$= 7.96 μm. At a photonic stop band, one expects to observe high optical reflectance. Figure 3(b) shows the reflectance spectra of the SP2 PC, obtained by FTIR testing (the blue curve) and by FDTD simulation for both x-polarized (the brown curve) and y-polarized (the red curve) incident waves. Their averaged value is indicated as the dashed green curve. The curves agree well, i.e., they both exhibit high reflectance at λ_{peak}= 7.1 μm and a full-width-half-maximum (FWHM) of Δλ~ 0.8 μm. λ_{peak} also agrees with $\lambda_{mid\text{-}gap}$, within 0.8μm. This agreement between FTIR testing and FDTD and dispersion calculations demonstrates the success of our optical lithographic system in fabricating a nearly ideal SP2 PC. However, the simulation peak reflectance for x-, y-polarized, and unpolarized incident waves are 85%, 50% and 67.5%, respectively. The measured peak reflectance is 50%, which is slightly lower than the averaged FDTD value of 67.5%. The slightly reduced experimental reflection at λ = 7.1 μm may be due to optical scattering by local structure roughness, fabrication imperfections or non-straight sidewalls.

To improve the optical performance and increase reflection at the photonic stop band, we performed material inversion of the SU8-based SP2 PC to transform it into a Cadmium Sulfide (CdS)-based structure. CdS has a higher optical index (n = 2.5) than SU-8 and should give a wider photonic stop band. To perform the inversion, we first deposited CdS throughout the entire SP2 PC structure and then performed a series of etch steps to burn away the SU8 scaffolding. The experimental challenge is to apply a conformal CdS coating to the SU8-template such that the PC structure integrity is not distorted. This coating maybe done using a low temperature chemical-vapor-deposition (CVD) method. Figure 4(a)–(d) shows a sequence of SEM images of CdS conformal coating on an SU8-based SP2 PC. Figure 4(a) shows an SEM image of a uniform, planar CdS coating on an SiO_2 substrate. Figure 4(b) shows an SEM image of a conformal coating of CdS throughout the 3D structure. The coating gives a similar CdS thickness on the top (H_2=286nm), along the side (V_2=294nm) and at the bottom (H_3=310nm) of the SU8 slanted rods. The average coating thickness is t = (294 ± 8) nm. Figure 4(c) shows an SEM image at a different viewing angle to display the way the slanted rods cross each other. Again, the CdS coating is conformal and does not alter the tilt angle (θ = 45°) of the slanted rods. Figure 4(d) shows an SEM image of the CdS coating on a 2 unit-cell SP2 PC, which is also conformal over the entire structure.

After the CdS deposition, we perform a sequence of etching steps to remove the SU8 template. The details are described in the Method section. Once the SU8 template has been removed, we have realized an inverted SP2 PC structure. The new SP2 PC now consists of mutually crossing air pores in a CdS background. Figure 4(e) shows the reflectance spectra of the CdS-based SP2 PC, obtained by both FTIR measurement (the blue curve) and by FDTD simulation (the red curve). The FTIR data shows a high reflectance of

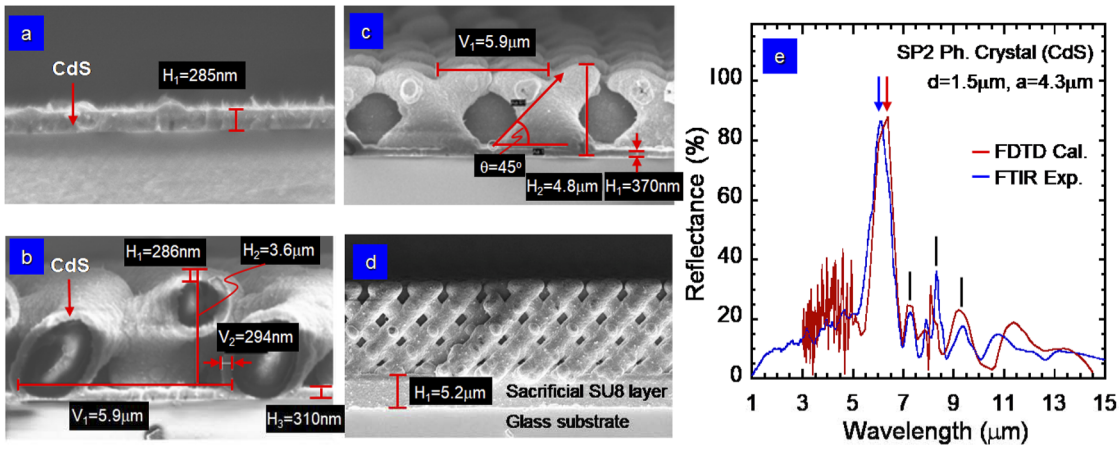

FIG. 4. (a)-(d) are SEM images of a conformal coating of CdS onto a SU8-based SP2 photonic crystal. (a) shows a uniform coating of a planar layer of CdS; (b) shows a conformal coating of CdS layer throughout the 3D structure. The coating gives a similar CdS thickness on the top and along the side of the SU8 slanted rods; (c) shows that CdS coating is conformal and also does not alter the tilt angle of the slanted rod; (d) shows CdS coating to a 2 unit-cells SP2 PC, which is also conformal over the entire SP2 PC structure. (e) Reflectance spectra of the Air pore in CdS background SP2 with d = 1.5μm. The experimentally measured curve (blue color) are compared to a FDTD simulation result (red color). The reflectance peak at λ=6.1μm corresponds to a normalized frequency of 0.70 (c/a).

R~85% at λ_{peak}=6.1 μm. The FDTD curve likewise shows a high reflectance of R~85% at λ_{peak} = 6.3 μm. There is a good agreement of the peak wavelength between the two curves. The fact that both spectra exhibit a high reflectance of ~85% at λ_{peak}, indicates the existence of a large photonic stop band along ΓZ. At the reflectance peak, the FWHM is Δλ~0.9 μm or, equivalently, a gap-to-midgap ratio of Δλ/λ ~15%. It maybe concluded that the use of a higher index material, such as CdS, produces a slightly wider and more robust photonic stop band. Note also that even the side peaks at λ~7.2, 8.3 and 9.3 μm agree with each other between the FTIR and FDTD simulation.

In addition to coating a semi-conducting material such as CdS, a metallic coating is also an effective way to modify the optical properties of the SU8-based SP2 PC. As an example, we use atomic-layer-deposition (ALD) to coat a thin layer of Platinum (Pt) onto our SU8 PC. The ALD Pt conformally coats the SU8-based SP2 PC at a rate of 0.1 nm/min. Additionally, since the skin depth of Platinum t is 10-30 nm for λ=1-10 μm, a thin Pt coating is sufficient for optical index modification. Figure 5(a) shows an SEM image of a uniform, planar Pt coating. The thickness is t = 65 nm. Figure 5(b) shows an SEM image of a conformal Pt coating on a unit-cell (one cross) SU8-based SP2 PC. The SU8 slanted rod is surrounded by a thin layer of

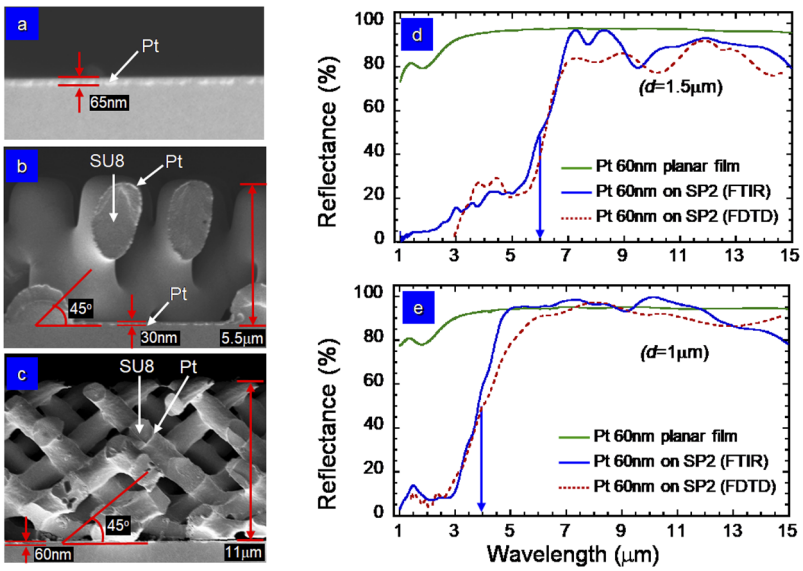

FIG. 5. (a)-(c) are SEM images of a conformal coating of Platinum (Pt) onto a SU8-based SP2 photonic crystal. (a) shows a uniform coating of a planar layer of Pt; (b) shows a conformal coating of Pt throughout a unit-cell (one cross) of SU8-based photonic crystal; (c) shows conformal Pt coating to a 2 unit-cells SP2 PC. (d) and (e) are reflectance of SU8 in air background SP2 PC structure, coated conformally with 60nm Pt with d = 1.5μm and 1μm, respectively. The green curves are the reflectance spectra of Pt 60nm planar film. The curves with red color are the FDTD simulation results, and the curves with blue color are the experimental data from FTIR measurement.

Pt coating. On top of the substrate, a thin Pt layer of t = 30 nm is also visible. Figure 5(c) shows an SEM image of a conformal Pt coating throughout a 2 unit-cell SP2 PC.

Figure 5(d) show the reflectance spectra of the Pt-coated SP2 PC, obtained by both FTIR testing and FDTD simulation. The PC sample has a rod width d = 1.5 μm and a lattice constant a = 4.3 μm. In our FDTD computation, Pt is modeled using the data from Ref. 29 and implemented according to the dispersion model of MEEP materials library.[30] We also assume a 60nm thin Pt layer on the substrate, as shown in Fig. 5(c). The reflectance spectrum of a Pt planar film of t = 60 nm is also shown as a reference (the green curve). It exhibits a high reflectance (R>90%) for a wide range of infrared wavelengths from λ = 3–15μm. The FTIR data (the blue curve) show a low reflectance (R<20%) for λ = 1–5 μm and a high reflectance (R>90%) for λ = 7–15 μm. At the photonic band edge around λ~6 μm, there is a sharp rise in reflectance that indicates the onset of a plasmonic band gap. The FDTD result (the red curve) agrees well with the FTIR data, which also shows a photonic band edge at λ~6μm. To illustrate the length-scaling behavior of our Pt-coated SP2 PC, we fabricated a new sample with reduced characteristic dimensions and studied its optical properties. Figure 5(e) shows the reflectance spectra of the Pt-coated SP2 PC, having d = 1.0 μm and a = 2.92 μm. The FTIR, FDTD, and planar Pt film data are shown as blue, red, and green curves, respectively. The FTIR data exhibit a low reflectance (R<10%) for λ=1–3 μm, a sharp rise of reflectance at λ = 4 μm and a high reflectance at λ = 5–15μm. Note that the observed photonic band edge shifted from λ= 6 μm to 4 μm, when the rod diameter was reduced from d = 1.5 μm to 1.0 μm. This validation of linearly scaling behavior shows that the observed photonic band edge originates from the photonic crystal band structure. Again, the experimental FTIR data agrees well with the FDTD simulation result. It is noted that, in our optical lithographic system, it is relatively easy to create SP2 PCs of different lattice constants by changing the dimensions of the optical mask. Note also that a metallic PC having a low reflectance of R~10% for λ = 1-3μm and a correspondingly high absorptance A~90% can function as a spectrally selective emitter for an energy efficient thermo-photovoltaic applications.[31]

IV. CONCLUSIONS

In summary, we proposed and demonstrated an off-axis optical lithographic method to make 3D SP2 PCs that is inherently low-cost and wafer-scale. The lithographic steps are simple and fast, involving two off-axis optical exposures and a precision shifting of the optical mask. Additionally, the instrumentation is low cost, as its major components consist of a laser, a prism, an optical mask and a precision translational stage. Through a detailed process calibration, we have shown that a nearly perfect SP2 PC can be fabricated, having a minimum feature size of d = 1.0 μm and a large sample size of 8x10 mm^2, without any observable fabrication defects. Particularly, three different types of SP2 PC were successfully created: (i) SU8 posts in air background, (ii) air pores in CdS background and (iii) Pt coated on SU8 SP2 templates. The optical performances of the SP2 PCs were studied by FTIR reflectance measurements. The experimental results agree with those obtained from a FDTD simulation and a dispersion calculation. The agreement indicates that the fabricated 3D PC has the desirable lattice symmetry, dimensions and the designed optical properties. We believe this low-cost and large-scale method could enable a broader technological impact and future utilization of 3D PC materials. Furthermore, this off-axis method is unique and could lead to the creation of an entirely new class of slanted-rod based photonic crystals, such as the recently proposed topological photonic crystal in 3D.[32]

V. METHODS

A. Theoretical modeling of the frequency-wavevector dispersion

The dispersion diagrams are calculated using plane-wave expansion method, implemented through an open-source software package MIT Photonic Bands (MPB).[33] The unit cell of the SP2 PC consists of two pores, slanted at +45° and −45° angles, respectively. Figure 1(b) shows the primitive vectors spanning the PC in the xy-plane and are denoted by $\vec{a}_1$ and $\vec{a}_2$, respectively. From the given geometry, these two primitive vectors can be calculated as, $\vec{a}_1 = a(\cos\alpha, \sin\alpha, 0)$ and $\vec{a}_2 = a(\cos\alpha, -\sin\alpha, 0)$, where α is the angle between $\vec{a}_1$ and x-axis. For an inter-pore angle 90 degree, the third lattice vector $\vec{a}_3$ can be evaluated according to Ref. 28 as, $\vec{a}_3 = (0, 0, c)$, where $c = 1.4552a$.

B. Theoretical modeling of finite-difference-time-domain (FDTD)

The FDTD computations are performed using a free, open-source software package, MIT Electromagnetic Equation Propagation (MEEP).[34] The unit cell used for the FDTD computations is shown by the highlighted green square in Fig. 1(b). Periodic boundary conditions (PBC) are applied along x and y-directions. The SP2 PC is assumed to have two unit cells along z-direction and rests on a 2 μm-thick SiO_2 substrate (refractive index 1.45). The top of the SP2 PC is padded with air region of height 8c. The top of the air region and the bottom of the SiO_2 substrate is terminated by perfectly matched layers (PML). Effectively, this simulates a semi-infinite substrate. The PC is illuminated with a normally incident, x-polarized and y-polarized plane wave coming from +z -direction.

C. Fundamental optical limit of the size and depth of the slanted posts

The laser lithographic method we proposed in this paper requires the use of a 2D mask during optical exposure. The size and shape of the produced slanted post is defined by the laser beam profile after it passes through the 2D mask. By the scalar diffraction theory, the laser beam profile is influenced by the aperture's diameter (d) on the mask, the laser wavelength (λ) and also the laser propagating depth (z) into the photoresist. To maintain a well collimated beam profile, we use the Fresnel number ($N_F = \frac{d^2}{z\lambda}$) to describe the limit of our optical system. Therefore, as d is reduced, z or λ has to be reduced accordingly to produce a slanted post with a uniform diameter. Our initial experimental data supports this reasoning. For example, in our experiment of making 3D SP2 structure, when d=1.5μm and λ=355nm, we observed uniform post diameter up to a thickness of z=14μm. The deduced Fresnel number is 0.66. For d=1μm and λ=355nm, we found z=6μm, and the corresponding

N_F=0.64. Therefore, for a given λ used for the optical system, the minimum achievable d is set by $N_F = \frac{d^2}{z\lambda} \sim 0.64 - 0.66$.

D. SP2 SU8 sample preparation and development

The SU8 photoresist was spin-coated on 1 mm thick SiO_2 substrates. The typical thickness of the SU8 layer varied from ~20 μm at 1000 rpm, to ~10 μm at 3000 rpm. The SU8 samples were then baked on a hot plate at 95 °C for 1 to 2 minutes to remove residual solvent. After the UV exposure, the SU8 samples were baked again at 95°C for 1–2 minutes (post exposure bake), then dipped in SU8 developer for 1–2 minutes and rinsed with IPA.

E. Low temperature CdS deposition on 3D SU8 photonic structures by CVD

A home-built horizontal hot-wall metalorganic chemical vapor deposition (CVD) reactor was used for the conformal deposition of CdS thin films on SU8 photonic crystal structures. Ultra-high purity (UHP) hydrogen was used as the carrier gas. Dimethylcadmium (DMCd) and hydrogen sulphide (H_2S diluted with hydrogen) were used as the sources for cadmium and sulphur, respectively. The hot-wall configuration consists of two clamshell heaters wrapped around a 4-inch internal diameter quartz reactor. All depositions were carried out with the susceptor temperature maintained at about 50 °C with the help of both front and back heaters set to 80°C. Precursors carried by UHP H_2 enter the reactor zone and undergo the chemical reaction $(CH_3)_2Cd + H_2S \rightarrow CdS + 2CH_4$ to deposit uniform CdS thin films on the photonic structures.

F. Pt deposition on 3D SU8 photonic structures by ALD

The deposition of platinum was performed in an Arradiance ALD system, strictly alternating exposure of two different precursors on the surface which then slowly forms a thin film. First, the system was heated up to 250°C, followed by a 1 nm Al_2O_3 nucleation layer, and then bulk platinum was deposited. A total platinum thickness of 60 nm was done in two 8.5 hour sessions, where the nucleation layer took 10 cycles and 30 nm of platinum took 300 cycles for each session.

G. Removal of SU8 PC template after CdS deposition

Optimization of the photonic band gap of the SP2 structure requires the removal of the SU-8 polymer template following the deposition of CdS. To expose the template, we used a Trion Phantom series ICP-RIE system to dry etch the CdS overlayer in an 8:1 H_2/CH_4 plasma at a pressure of 25 mTorr, resulting in a linear etch rate of 77.6 ± 2.8 nm/min. The top 12 microns of the template is then removed in the same etching system by infiltrating the template with oxygen. Because oxygen infiltration becomes more difficult further into the structure, the template was removed non-linearly, and we found that the top 6 microns was removed at about 50 nm/min, while the next 6 microns was removed at about 17 nm/min. After 8-10 hours, exposure to oxygen no longer removed the template, so the inversion process was completed by burning off the remaining SU-8 in a furnace at 450°C. Because SU-8 is used as an underlayer to promote adhesion of the templates to the substrate, the time in the furnace was limited to 15 minutes, which was sufficient to remove the last few microns.

ACKNOWLEDGMENTS

MLH acknowledges financial support from MOST 105-2221-E-009-111-MY3 and also international travel support from DOE-BES. S.Y.L. gratefully acknowledges financial support from NSF under award ECCS-1840673-NOA. S.J. gratefully acknowledges partial financial support from DOE Office of Science under award DE-FG02-06ER46347.

REFERENCES

[1] S. John, "Strong localization of photons in certain disordered dielectric superlattices," Phys. Rev. Lett. **58**, 2486 (1987).
[2] E. Yablolnovitch, "Inhibited spontaneous emission in solid-state physics and electronics," Phys. Rev. Lett. **58**, 2059 (1987).
[3] J. D. Joannopoulos, P. R. Villeneuve, and S. Fan, "Photonic crystals: Putting a new twist on light," Nature **386**, 143–149 (1997).
[4] A. Chutinan, S. John, and O. Toader, "Diffractionless flow of light in all-optical microchips," Phys. Rev. Lett. **90**, 123901 (2003).
[5] S. Y. Lin, J. G. Fleming, D. L. Hetherington, B. K. Smith, R. Biswas, K. M. Ho, M. M. Sigalas, W. Zubrzycki, S. R. Kurtz, and J. Bur, "A three-dimensional photonic crystal operating at infrared wavelengths," Nature **394**, 251 (1998).
[6] M. Bayindir, E. Ozbay, B. Temelkuran, M. M. Sigalas, C. M. Soukoulis, R. Biswas, and K. M. Ho, "Guiding, bending, and splitting of electromagnetic waves in highly confined photonic crystal waveguides," Phys. Rev. B **63**, 081107 (2001).
[7] S. Y. Lin, E. Chow, H. Vince, P. R. Villeneuve, and J. D. Joannopoulos, "Experimental demonstration of guiding and bending of electromagnetic waves in a photonic crystal," Science **282**, 274 (1998).
[8] E. Chow, S. Y. Lin, S. G. Johnson, J. D. Joannopoulos, J. R. Wendt, G. A. Vawter, W. Zubrzycki, H. Hou, and A. Alleman, "Three-dimensional control of light in a 2D photonic crystal slab," Nature **407**, 983–986 (2000).
[9] J. D. Joannopoulos, R. D. Meade, and J. N. Winn, *Photonic Crystal: Molding the flow of light* (Princeton University Press, Princeton, NJ, 1995).
[10] K. Sakoda, *Optical Properties of Photonic Crystals* (Springer-Verlag New York, LLC, 2001).
[11] B. Frey, P. Kuang, M.-L. Hsieh, J.-H. Jiang, S. John, and S.-Y. Lin, "Effectively infinite optical pathlength created by simple-cubic photonic crystal for extreme light trapping," Scientific Report **7**, 4171 (2017).
[12] G. Demesy and S. John, "Solar energy trapping with modulated silicon nanowire photonic crystals," J. App. Phys. **112**, 074326 (2012).
[13] There are many important approaches that are based on the bottom up approaches. Some of the representative references are listed in the following. V. L. Colvin, "From opals to optics: Colloidal photonic crystals," MRS Bulletin **26**, 637 (2001); W. L. Vos and A. Polman, "Optical probes inside photonic crystals," *ibid.* **26**, 642 (2001).
[14] S. Y. Lin, J. G. Fleming, and E. Chow, "Two- and three-dimensional photonic crystals built with VLSI tools," MRS Bulletin **26**, 627 (2001).
[15] S. Noda, "Two- and three-dimensional photonic crystals in III-V semiconductors," MRS Bulletin **26**, 618 (2001).
[16] K. M. Ho, C. T. Chan, C. M. Soukoulis, R. Biswas, and M. Sigalas, "Photonic band gaps in three dimensions: New layer-by-layer periodic structures," Solid State Commun. **89**, 413 (1994).
[17] E. Ozbay, E. Michel, G. Tuttle, R. Biswas, M. Sigalas, and K. M. Ho, "Three-dimensional simple cubic woodpile photonic crystals made from chalcogenide glasses," Appl. Phys. Lett. **64**, 2059 (1994).
[18] S. Noda, K. Tomoda, N. Yamamoto, and A. Chutinan, "Full three-dimensional photonic bandgap crystals at near-infrared wavelengths," Science **289**, 604 (2000).

[19]K. Aoki, H. T. Miyazaki, H. Hirayama, K. Inoshita, T. Baba, K. Sukoda, N. Shinya, and Y. Aoyagi, "Microassembly of semiconductor three-dimensional photonic crystals," Nat. Mater. **2**, 117 (2003).
[20]O. Toader, M. Berciu, and S. John, "Photonic band gaps based on tetragonal lattices of slanted pores," Phys. Rev. Lett. **90**, 233901 (2003).
[21]J.-H. Jiang and S. John, "Photonic architectures for equilibrium high-temperature Bose-Einstein condensation in dichalcogenide monolayers," Sci. Rep. **4**, 7432 (2014).
[22]M. Deubel, M. Wegener, A. Kaso, and S. John, "Direct laser writing and characterization of slanted pore photonic crystals," Appl. Phys. Lett. **85**(11), 1895 (2004).
[23]N. Tetrault, G. V. Freymann, M. Deubel, M. Hermatschweiler, F. Perez-Willard, S. John, M. Wegener, and G. A. Ozin, "New route to three-dimensional photonic bandgap materials: Silicon double inversion of polymer templates," Adv. Mater. **18**, 457 (2006).
[24]J. D. Williams, P. Sun, W. C. Sweatt, and A. R. Ellis, "Metallic-tilted woodpile photonic crystals in the midinfrared," J. Micro/Nanolith. MEMS **9**(2), 023011 (2010).
[25]L. Tang and T. Yoshie, "Woodpile photonic crystal fabricated in GaAs by two-directional etching method," JVST B **28**, 301 (2010).
[26]A. J. Turberfield, "Photonic crystals made by holographic lithography," MRS Bulletin **26**, 632 (2001).
[27]M.-L. Hsieh and S.-Y. Lin, "A compact holographic lithography system for photonic crystal structure," J. Vacuum Science and Technology B **29**, 011015 (2011).
[28]O. Toader and S. John, "Slanted-pore photonic band-gap materials," Phys. Rev. E **71**, 036605 (2005).
[29]A. D. Rakic, A. B. Djurisic, J. M. Elazar, and M. L. Majewski, "Optical properties of metallic films for vertical-cavity optoelectronic devices," Applied Optics **37**, 5271–5283 (1998).
[30]MEEP materials library, https://github.com/stevengj/meep/blob/master/python/materials.py.
[31]S. Y. Lin, J. Moreno, and J. G. Fleming, "A 3D photonic-crystal emitter for thermal photovoltaic generation," Appl. Phys. Lett. **83**, 380 (2003).
[32]L. Lu, C. Fang, L. Fu, S. G. Johnson, J. D. Joannopoulos, and M. Soljacic, "Symmetry protected topological photonic crystal in three dimensions," Nature Physics **12**, 337 (2016).
[33]S. G. Johnson and J. D. Joannopoulos, "Block-iterative frequency-domain methods for Maxwell's equations in a planewave basis," Optics Express **8**, 173–190 (2001).
[34]A. F. Oskooi, D. Roundy, M. Ibanescu, P. Bermel, and J. D. Joannopoulos, "Meep: A flexible free-software package for electromagnetic simulations by the FDTD method," Computer Physics Communications **181**, 687–702 (2010).